NASA PURCHASE ORDER: S-30943-F (ARC # 1296)
TITLE: A Search for EUV Emission from the O4f Star Zeta Puppis
PRINCIPLE INVESTIGATOR: Dr. Wayne L. Waldron (Applied Research Corporation)
CO-INVESTIGATOR: Dr. John Vallerga (Eureka Scientific, Inc.)
SUBJECT: EUVE Final Report
PO START DATE: 16 March 1995
OBSERVATION START DATE: 20 December 1995
DELIVERY DATE: 12 November 1996

ABSTRACT

We obtained a 140 ks EUVE observation of the O4f star, ζ Puppis. Because of it's low ISM column density and highly ionized stellar wind, a unique EUV window is accessible for viewing between 128 to 140 Å, suggesting that this star may be the only O star observable with the EUVE. Although no SW spectrometer wavelength bin had a signal to noise greater than 3, a bin at 136 Å had a signal to noise of 2.4. This bin is where models predict the brightest line due to OV emission should occur. We present several EUV line emission models. These models were constrained by fitting the ROSAT PSPC X-ray data and our EUVE data. If the OV emission is real, the best fits to the data suggest that there are discrepancies in our current understanding of EUV/X-ray production mechanisms. In particular, the emission measure of the EUV source is found to be much greater than the total wind emission measure, suggesting that the EUV shock must produce a very large density enhancement. In addition, the location of the EUV and X-ray shocks are found to be separated by ~ 0.3 stellar radii, but, the EUV emission region is found to be ~ 400 times larger than the X-ray emission region. We also discuss the implications of a null detection and present relevant upper limits.

1. INTRODUCTION

The X-ray production mechanism in OB stars has been a subject of debate for over a decade. The basic discriminator between the proposed models is the spatial location of the X-ray source within the surrounding stellar wind (for a general discussion of these models see Cassinelli 1985). As discussed below, extreme ultraviolet (EUV) observations have the potential to resolve this issue. To determine this location one must include two sources of X-ray attenuation: (1) the interstellar medium (ISM), and; (2) the stellar wind. In the massive stellar winds of O stars, the total wind column density (N_w) is much greater than the ISM column density (N_{ISM}). However, since these winds are highly ionized, specific energy ranges can be dominated by either the wind or ISM. For example, in early O stars, where Helium is almost completely ionized, the stellar wind component dominates the ISM shortward of ~ 130 Å, and is essentially transparent longward of 130 Å, where in this range the absorption is controlled by the ISM.

The importance of determining the X-ray location is fundamental in establishing the intrinsic strength of the X-ray emission with regards to the total stellar energy. If the X-rays are deeply embedded within the wind (total N_w), as suggested by Cassinelli & Olson (1979), the ratio of the intrinsic X-ray flux to stellar flux is of the order of 10^{-3} (Waldron 1984). Whereas, if the X-rays are produced by shocks due to the unstable nature of radiative driven winds, as proposed by Lucy & White (1980), and since these shocks can only occur in the outer regions of the wind (Owocki, Rybicki, & Castor 1988), where only a small fraction of the total N_w contributes to the wind absorption, the intrinsic X-ray flux will only be slightly larger than the observed value (10^{-7} times the stellar flux).

The astrophysical significance is obvious. First, if the X-rays are proven to be totally due to shocks, then the problem is

solved, i.e., we know the mechanism and location. On the other hand, if we find evidence supporting deeply embedded X-ray emission, then, we may ask, what is the mechanism responsible for this large emission, and how do we confine this high density hot plasma; are there magnetic loops on OB stars? At first, since, OB stars do not possess a significant outer convection region, the concept of magnetic loops is questionable. However, over the past several years, studies of magnetic field effects in these stars suggest that these fields may no longer be ignored (see discussion by Cassinelli 1992). For example, the HEAO-2 SSS analysis by Cassinelli & Swank (1983) found evidence for very high temperature gas (> 15 x 10^6K) and they suggested that this gas may be confined in magnetic loops. Recent ASCA SIS observations of OB stars (Corcoran et al. 1994; Cohen et al. 1996) confirm that very high temperature gas is present (10 - 30 x 10^6K), and the emission is thermal as evident by the presence of X-ray lines. Furthermore, since these stars possess various mechanical catalysts (rapid rotation, differential rotation, and non-radial pulsations), along with the strong radiative force, the complex physics involved will require new and innovative approaches to studies of gas dynamics. Clearly, any hint of hot/warm, high density plasma will provide the incentive to continue these studies.

Another question we must address, is there any strong evidence that stellar wind absorption is important? Waldron (1991) found a strong correlation between the X-ray hardness ratios (indicators of X-ray absorption) and the 6 cm radio data (a direct measure of N_w) in O stars, suggesting that the degree of X-ray attenuation is highly influenced by the surrounding stellar wind envelope. He also pointed out that the best fits from the automated HEAO-2 IPC processing (ISM absorption only) for O stars imply that an additional X-ray absorption mechanism must be present. This has also been noted in fitting the limited BBXRT spectra (Corcoran et al. 1993), and in fitting high signal to noise ROSAT PSPC spectra (Hillier et al. 1993). The presence of wind absorption has been confirmed by our ASCA O star observations (Corcoran et al. 1994), and the ASCA PV phase observation of ς Puppis reported by White (1996).

Unfortunately, the X-ray data (e.g., HEAO-2, ROSAT, and ASCA) alone are not sufficient to determine the spatial location of the X-rays. For example, from X-ray temperature versus absorption column density plots (so-called "banana plots", see Cassinelli et al. 1981), the range of acceptable fits range a decade in temperature and typically three decades in column density. Although X-ray data from ROSAT (see discussion below) and ASCA have proven to be very useful in improving this wide range of acceptable fits, a null or positive detection of EUV emission will provide fundamental key pieces to the puzzle.

2. SCIENTIFIC GOAL AND EUVE TARGET SELECTION

We proposed to use the Extreme Ultraviolet Explorer (EUVE) short wavelength (SW) Spectrometer to search for low temperature (< 500,000K), high volume emission measure (EM ≈ 10^{58} cm^{-3}) plasma in O stars. In order to observe EUV emission in O stars three stringent conditions must be satisfied; (1) the O star must have a highly ionized wind (He almost completely ionized); (2) the ISM column density (N_{ISM}) must be ≤ 10^{20} cm^{-2}, and; (3) to overcome the still rather large optical depth (≈8), the EUV emission measure must be quite large, EM > $10^{58}$$cm^{-3}$. This EM is not unreasonable for deeply embedded X-ray sources (e.g., Waldron 1984).

However, since most O stars suffer from fairly large ISM absorption with ISM column densities > $5x10^{20}$ cm^{-2}, our choice of targets is highly restricted. We believe that the best EUVE O star target is the unredden O4f star, ς Puppis. Historically, this star has served as the benchmark for testing various stellar wind models. Except for the EUV, it has been observed extensively in the radio through X-ray spectral bands. It is unique among the O stars for two reasons: (1) it has a low ISM column density (N_{ISM} = $9.8x10^{19}$ cm^{-2}), and; (2) it is hot enough such that its stellar wind opacity is essentially transparent longward of ~ 130 Å. For ς Puppis this combination of low ISM absorption and small wind opacity produces an EUV window between 128 - 140 Å (a small region of the SW band) where the EUV optical depths are less than 10 as illustrated in Figure 1. The EUV optical depths shown in Figure 1 are the results of fitting the PSPC

X-ray spectrum of ς Puppis (see discussion in Sec. 3). This window is a direct consequence of the influence of EUV and X-ray emission on the overlying wind opacity structure as discussed by Waldron (1984).

3. CONSTRAINTS ON EUV EMISSION FROM X-RAY DATA

For O stars, the IPC X-ray data yield a wide range of acceptable fits (assuming Raymond-Smith X-ray spectra); for $N_w \approx 0$, we find acceptable fits require a log T ≈ 7.0 and log EM (emission measure) ≈ 55, and; for full wind attenuation, we find a log T ≈ 6.6 and log EM ≈ 57.5 are required (Cassinelli et al. 1981; Waldron 1984). Although these two limiting cases alone cannot produce enough EUV radiation to be detected by the EUVE, we suggest that in addition to the T and EM stated above, a second low T (or a distribution of low T components), higher EM plasma is also present. This is not unreasonable since in reality any X-ray source more than likely has a continuous distribution of T and EM (e.g., the sun's transition region). For example, according to the shock model of Owocki et al. (1988), the density can change by an order of magnitude within a given shock. The detailed T structure was not determined, but should react in some predictable manner. For a deeply embedded X-ray source, a continuous distribution in T and EM is naturally expected since this is where the density is changing rapidly. This type of structure was used by Wolfire, Waldron, & Cassinelli (1985) to illustrate the compatibility of a thin coronal zone with the IR excess observed (IRAS) in ς Puppis.

Cohen et al. (1994) found that B star models compatible with EUV and X-ray emission require a distribution of temperatures with the corresponding EM scaling as T^{-1}. In addition, our ASCA SIS observations confirm that multiple temperatures are a necessity in fitting O star spectra (unfortunately ASCA data are not very useful for constraining EUV emission since the low energy cutoff is approximately 0.4 keV). Therefore, the probability is high that low T, high EM plasma may exists in the outer atmospheres of O stars.

Hillier et al. (1993) obtained a very high signal to noise PSPC observation of ς Puppis. Since the PSPC is more sensitive to softer X-rays (< 0.2 keV), as compared to the IPC and ASCA instruments, this observation allows us to obtain constraints on the soft EUV emission component. Hillier et al. claim that their best fit (reduced $\chi^2 = 11$) to the data required two temperatures (log T = 6.23 and 6.66) and a complex wind opacity distribution. We find, using a stellar wind opacity described by Waldron (1984), that a significantly better fit (reduced $\chi^2 = 2.8$) can be obtained with a single T, single N_w, model (log T = 6.57, log N_w = 22.09, log EM = 56.97). In principle, for standard spherical symmetric wind conditions, and a known mass loss rate, N_w can be used to establish the location of the X-ray emission, and EM can be compared with the total wind emission measure, EM_w, to determine the relative strength of the X-ray emission to the total available wind emission, as described by Cassinelli et al. (1981). Adopting the stellar parameters from Lamers & Leitherer (1993) (mass loss rate = 2.4×10^{-6} solar mass/year, stellar radius = 16 solar radii, and v_∞ = 2400 km s^{-1}) and a velocity law of the form $v(r) = v_\infty(1-r_o/r)^{0.8}$, the X-ray best fit N_w suggests that the position of the X-ray source is at 2.23 stellar radii (or in velocity units, 0.62 v_∞). This is consistent with the findings of MacFarlane et al. (1993) where the X-rays were constrained by UV observations. For ς Puppis, the log EM_w = 58.63 (measured from $0.1v_\infty$ to v_∞) yielding a $EM/EM_w = 0.022$, suggesting that the X-ray emission represents a small perturbation in the stellar wind, consistent with the shock scenario.

To establish constraints on the EUV emission, we include an EUV low temperature component in our fitting procedure. This component is parameterized by an EUV T (T_{EUV}), EM (EM_{EUV}), and N_w (N_{EUV}). Both components assume Raymond & Smith (1977) emissivities in the calculation of the EUV and X-ray emission. All models use the ISM cross sections of Morrisson & McCammon (1983) and assume a fixed ISM column density of 9.8×10^{19} cm^{-2}. We find that the X-ray component predicted from this two component fit remains identical to the single T fit, and the EUV component adds a very minor adjustment to the low PSPC bins. The best fit to the X-rays, consistent with our EUVE observations, is shown in Figure 2. Notice that the EUV component's contribution is very small, and the significance of this

component could only be achieved because of the very high signal to noise PSPC observation (the EUV best fit model is discussed in Section 5).

From a statistical point of view, the fact that the EM_{EUV} (i.e., second component scale factor) is not determined to be zero implies that the X-ray data is slightly improved by the presence of an EUV component which is evident by the total χ^2 which are slightly better than the single component fit, but the reduced χ^2 are slightly larger due to the reduction in degrees of freedom (DOF). These fits represent the minimum N_{EUV} and EM_{EUV} that yield the minimum χ^2. Beyond these minimum values we find that further increases in N_{EUV} and EM_{EUV} do not change the minimum χ^2, suggesting that the true EUV emission component could be larger, i.e., a significantly larger EUV component could be present at deeper layers in the stellar wind. Hence, the results presented here should be considered as the minimum EUV properties consistent with the X-ray spectrum.

Several models were calculated and the EUV parameters of these multiple component fits are tabulated in Table 1. The EUV luminosities (erg s^{-1}) represent the total EUV energy in the wavelength range 75 to 150 Å. For comparison, the corresponding logs of the intrinsic and observed X-ray luminosities are respectively 33.77 and 32.50. The column EM_{EUV}/EM_W shows that all models predict $EM_{EUV} > EM_W$. The columns V_{EUV} and R_{EUV} give the velocity (normalized to v_∞) and radial (in stellar radii) positions of the EUV source. The line emission columns show the predicted EUVE counts for the strongest lines in the 128 to 140 Å range corresponding to OVI (130.3 Å), FeVIII (131.2 Å), MgV & OVI (132.6 Å), and OV (135.9 Å). Several emission line models are shown in Figure 3. In Figures 4 & 5, the strength of these lines as a function of T_{EUV} (Fig. 4) and wind velocity or equivalently wind position (Fig. 5) are presented.

4. EUVE OBSERVATIONS

We obtained a 140 ks observation of ς Puppis during the period 20 December 1995 to 25 December 1995. The observation was offset 0.11 along the positive X axis. John Vallerga's (Co-Investigator) primary role in this investigation involved special planning of the observation and the initial reduction and analysis of the raw data. Once analyzed, a fluxed spectrum was forwarded to the Principal Investigator for his detailed analysis and comparison with his models of the EUV flux expected from a star of this type.

As expected, since the observed signal was relativity weak, it was essential that all techniques be used in the data reduction process to enhance the signal to noise of the observation. Using the standard EUV packages in IRAF, the first step was to reduce the Deep Survey direct imaging data. Because bright O and B stars are prodigious emitters of UV radiation and the Deep Survey instrument has a small but finite sensitivity to UV radiation (2200-2800 Å), the detection of this source image did not imply a 100 Å EUV detection but it did allow aspect correction. By determining the centroid of this image on a short timescale, we were able to correct the aspect determination to better than one arc minute and confirm we were observing the source. Given the new corrected aspect, the program CEP was run to remap detector events to the proper wavelength and position coordinates. These events were then time filtered to remove times of high background (SAA and dawn/dusk) as well as times where the source was occulted by the Earth. Finally, a pulse height filter was applied to the events. If the detector is in the so called OWSZO mode, the pulse height of each event is saved. Photon detector events define a narrow peak in pulse height while detector and particle background events tend to be distributed in an exponential function of pulse height. By defining a narrow pulse height window to the events, the signal to noise can be improved by up to 50%. This is dependent on the source of the background but in the SW spectrometer near the center of the MCP detector, background is dominated by intrinsic detector background plus high energy particle background. Once the remapped, filtered, full resolution spectral image was generated, inspection did not reveal any obvious spectrum across the two dimension image. A one dimensional strip was then extracted where the source should have been based on many previous observations with EUVE and providing enough

margin (a few extra pixels) for any systematic errors. An average background taken above and below the spectrum was subtracted in the standard way, keeping track of the statistical errors inherent in the process. The one dimensional spectrum was binned in the spectral direction such that the bins represented the typical spectral resolution of the SW spectrometer of 0.5 Å. The observed EUVE net counts are shown in Figure 6. Except for the very shortest wavelength bins at the edge of the detector where the background is high and changing very fast and background subtraction is unreliable, no wavelength bin had a signal to noise of greater than 3.

Intriguingly, a bin at 135.9 Å had a signal to noise of 2.4 which is where the models predicted the brightest line due to OV emission should occur. If this is a true detection, the EUVE counts are 16.8 ± 4.8 with a flux of $2.7 \times 10^{-4} \pm 1.1 \times 10^{-4}$ photons cm^{-2} s^{-1}.

5. DISCUSSION

Since we are dealing with a null or marginal EUVE detection, there are several possible explanations of the data. In this discussion we will focus on three possibilities. The first is based on the premise that the signal at 135.9 Å is a real detection, and the two component best fit models to the PSPC data are taken literally. The second also assumes the detection is real, but we consider modifications to the PSPC best fit models. The third is that we have a null detection.

5.a. Two Component Best Fit Model

The best fit EUV model parameters are log T_{EUV} = 5.18±0.02, log N_{EUV} = 22.165±0.020, log EM_{EUV} = 59.578±0.040, V_{EUV} = 0.565±0.015, and R_{EUV} = 1.96±0.06 (see Table 1). The predicted EUVE counts are compared with the observations in Figure 6 and the contribution of the EUV component to the PSPC spectrum is shown in Figure 2. The location of the EUV source is ~ 0.3 stellar radii below the X-ray source and separated in velocity space by ~ $0.06v_\infty$. The ratio of the EUV EM to the X-ray EM is ~ 405. Using the relationship between shock velocity and source temperature from MacFarlane & Cassinelli (1989), $Vs = 1000(T/1.3 \times 10^7)^{1/2}$ km s^{-1}, the shock velocities of the EUV and X-ray components are respectively 108 and 533 km s^{-1} which are consistent with the implied shock position velocities. However, the real problem with a shock definition is the relative strength of the two components (EM_{EUV}/EM). Since EM is proportional to the square of the density, this implies that the ratio of the EUV density to the X-ray density is ~ 20. Furthermore, estimating the size of the EUV shock as $0.05v_\infty$ (which is the maximum width in velocity space to avoid producing emission spikes in UV P Cygni line absorption troughs, which are not observed), the density enhancement of the EUV shock is 19 times the local density, indicating a very high compression factor, since the Rankine-Hugoniot continuity relation predicts a density jump at the EUV shock of only 1.1. Since detailed self-consistent shock models have not been developed to date, it is difficult to conclude whether such a shock scenario is plausible. This shock picture is similar to the model discussed by Krolik and Raymond (1985) where they suggest that these winds may possess both strong and weak shocks, with the weak shocks being responsible for the observed X-rays. The strong shocks occur deeper in the wind and produce mainly EUV radiation. In their model however, the separation between strong and weak shocks is much greater than the predictions of our models.

5.b. Modified Two Component Models

The best fit model is not the only possible explanation of the data. Recall that the best fits presented in Table 1 represent the minimum EM_{EUV} and N_{EUV}. There are a number of other possible combinations that could just as easily explain the observations. Assuming the OV emission at 135.9 Å is real, any log T_{EUV} between 5.2 and 5.5 could also be valid by reducing the EM_{EUV} to match the OV emission line (any reduction in EM_{EUV} for a given model will maintain or improve the χ^2). In Table 2 we show the resultant EM_{EUV}, EUV luminosities, and line counts, assuming that the OV

emission line counts are fixed at 16.8 (T_{EUV}, N_{EUV}, V_{EUV}, and R_{EUV} also remain fixed). This shows that any log T_{EUV} between 5.2 and 5.5 produces an acceptable fit to the EUVE SW spectrum. It is also evident that the EM_{EUV}/EM_W problem discussed in Sec. 4.a. is not as serve, where we see that for several T_{EUV}, $EM_{EUV}/EM_W < 1$. However, for log $T_{EUV} > 5.5$, the presence of a very strong Fe VIII (see Fig. 3) line would rule out these temperatures if the OV emission line is real, and the abundances are standard (ASCA observations suggest that abundances in O stars may be peculiar, e.g., Corcoran et al. 1994).

5.c. Null EUVE Detection

Based on the overall shape of the EUVE SW spectrum, the obvious conclusion is that we did not detect any EUV line emission. For this case, we derived a 3σ upper limit at 135.9 Å. The counts were divided by the effective area and effective exposure to give the spectral flux density at this wavelength to be 3.3×10^{-4} photons cm^{-2} s^{-1} (4.8×10^{-14} erg cm^{-2} s^{-1}), and the results tabulated in Table 2 should be interpreted as only upper limits. A null detection greatly reduces the probability that a coronal-type transition region exists at the base of these stellar winds.

6. CONCLUSION

Although our results cannot verify the existence of a warm T component based on the X-ray data and our low signal to noise EUVE observation, the EUV/X-ray fits suggest that the presence of a warm component is not completely ruled out. Due to the implications suggested by assuming a positive detection, we are continuing to re-analyze our EUVE data to determine whether a stronger signal to noise can be achieved. The results of this study are currently being prepared for submission to The Astrophysical Journal.

7. PREVIOUS EUVE OBSERVATION

We were granted a 60 ks EUVE SW Spectrometer observation of ς Puppis during the Cycle I phase, which, due to positional constraints, was not observed until November 1993. In addition, the observation suffered from a severe UV leak from two B stars (V magnitudes > 6). It was found that only 9 out of 31 night passes were obtained at the roll angle that removed the UV leak resulting in an effective exposure time of only 20 ks. We presented this discrepancy to Dr. Ron Oliversen (Deputy Project Scientist). He informed us that the problem was related to the catalogs used in the EUVE scheduling. Since the EUVE scheduling only checked for B star contamination down to 6th magnitude, the two stars that caused the contamination were not listed (the EUVE staff has determined that the two B stars are SAO 198848, V = 6.4 & SAO 198862, V = 8.3). We were told that this was an isolated incident and our proposed science was greatly effected because the contaminated high background would make it very difficult to detect the predicted faint line emission. This is shown in Figure 1 where we see that the expected signal is lost in the noise. In order to avoid this problem, the EUVE scheduling procedure has been modified to incorporate additional catalogs when searching for B stars in the field that go down to 10th magnitude. Dr. Oliversen agreed that our effective 20 ks observation did not allow us to carry out our scientific goal, and recommended that we should re-propose the observation at a significantly larger exposure. The final report was submitted 9 February 1995 (NASA Purchase Order # S-14648-F).

References

Cassinelli, J. P. 1992, in ASP Conf. Ser., "Nonisotropic and Variable Outflows from Stars", eds., L. Drissen, C. Leitherer, & A. Nota, Vol. 22, p. 134

Cassinelli, J. P. 1985, in Proceedings of the Hot Star Workshop NASA/GSFC: "The Origin of Non-Radiative Heating/Momentum in Hot Stars", eds., A. Underhill and A. Michalitsianos, (NASA CP-2358), p. 2

Cassinelli, J. P, & Olson, G. L. 1979, ApJ, 229, 304
Cassinelli, J. P., & Swank, J. H. 1983, ApJ, 271, 681
Cassinelli, J. P., Waldron, W. L., Sanders, W. T., Harnden, F. R., Rosner, R., & Vaiana, G. S. 1981, ApJ, 250, 677
Cohen, D. H., MacFarlane, J. J., Cooper, R. G., Sanders, W. T., Cassinelli, J. P., Drew, J. E., Vallerga, J. V., & Welsh, B. Y. 1994, preprint
Cohen, D. H., Cassinelli, J. P., & Waldron, W. L. 1996, preprint
Corcoran, M. F., Waldron, W. L., MacFarlane, J. J., Chen, W., Pollock, A. M. T., Torii, K., Kitamoto, S., Miura, N., Egoshi, M., & Ohno, Y. 1994, ApJ (Letters), 436, L95
Corcoran, M. F., et al. 1993, ApJ, 412, 792
Hillier, D. J., et al. 1993, A&A, 276, 117
Krolik, J. H., & Raymond, J. C. 1985, ApJ, 298, 660
MacFarlane, J. J., & Cassinelli, J. P. 1989, ApJ, 347, 1090
MacFarlane, J. J., Waldron, W. L., Corcoran, M. F., Wolff, M. J., Wang, P., & Cassinelli, J. P. 1993, ApJ, 419, 813
Morrisson, R., & McCammon, D. 1983, ApJ, 270,119
Lamers, H. J. G. L. M., & Leitherer, C. 1993, ApJ, 412, 771
Lucy, L. B., & White, R. L. 1980, ApJ, 241, 300
Owocki, S. P., Castor, J. I., & Rybicki, G. B. 1988, ApJ, 335, 914
Raymond, J. C., & Smith, B. W. 1977, ApJS, 35, 419
Waldron, W. L. 1991, ApJ, 382, 603
Waldron, W. L. 1984, ApJ, 282, 256
White, N. E. 1996, in, New Horizons in X-Ray Astronomy, ed. F. Makino, in press
Wolfire, M. G., Waldron, W. L., & Cassinelli, J. P. 1985, A&A, 142, L2

TABLE 1. EUV Best Fit Parameters

$\log T_{euv}$	$\log EM_{euv}$	$\log N_{euv}$	EM_{euv}/EM_w	V_{euv}	R_{euv}	EUV Luminosity (erg s^{-1})		EUV Line Emission (counts)			
K	cm^{-3}	cm^{-2}				intrinsic	observed	130.3	131.2	132.6	135.9
5.000	59.761	21.908	13.52	0.737	3.15	33.96	30.26	2.9	2.6	2.2	1.6
5.025	59.711	21.946	12.05	0.715	2.92	34.00	30.26	3.0	2.7	2.3	1.7
5.050	59.720	22.000	12.30	0.683	2.64	34.10	30.29	3.3	3.0	2.5	2.0
5.100	59.691	22.077	11.51	0.631	2.29	34.25	30.30	3.7	3.3	2.9	3.4
5.115	59.667	22.093	10.89	0.620	2.22	34.28	30.30	3.7	3.3	3.0	4.4
5.125	59.649	22.103	10.45	0.613	2.18	34.30	30.30	3.6	3.2	3.0	5.2
5.150	59.641	22.138	10.26	0.586	2.05	34.39	30.32	3.8	3.3	3.5	9.0
5.175	59.579	22.158	8.89	0.571	1.98	34.44	30.32	3.5	3.1	4.1	14.4
5.180	59.578	22.165	8.87	0.565	1.96	34.46	30.33	3.5	3.2	4.3	16.0
5.200	59.538	22.185	8.09	0.549	1.90	34.52	30.35	3.3	3.1	5.3	22.9
5.225	59.455	22.204	6.68	0.533	1.84	34.57	30.36	2.9	2.9	6.6	32.6
5.250	59.390	22.231	5.75	0.510	1.76	34.65	30.40	2.6	3.1	8.7	44.4
5.275	59.239	22.237	8.11	0.505	1.74	34.64	30.39	2.3	3.0	9.9	50.8
5.300	59.156	22.262	3.36	0.483	1.67	34.70	30.42	2.4	3.5	11.7	59.0
5.350	58.927	22.292	1.98	0.456	1.60	34.74	30.41	3.5	4.6	13.5	62.7
5.400	58.807	22.338	1.50	0.414	1.50	34.84	30.41	6.5	6.8	15.0	60.4
5.450	58.829	22.400	1.58	0.354	1.38	35.01	30.41	11.6	10.9	17.0	51.1
5.500	58.979	22.467	2.23	0.289	1.27	35.26	30.41	16.7	18.8	19.2	35.3
5.550	59.120	22.517	3.09	0.241	1.20	35.47	30.38	17.4	29.2	18.1	18.7
5.600	59.297	22.567	3.65	0.195	1.15	35.71	30.37	15.6	41.8	15.1	8.9
5.650	59.510	22.617	7.58	0.151	1.10	35.99	30.38	13.6	55.7	11.6	4.4
5.700	59.641	22.650	10.26	0.124	1.08	36.17	30.35	10.8	62.7	7.5	2.1
5.750	59.782	22.683	14.19	0.100	1.06	36.34	30.32	8.5	64.5	4.7	1.1

TABLE 2. EM_{EUV} Modified to Fit OV Emission Line

log T_{EUV}	log EM_{EUV}	EM_{EUV}/EM_{tr}	EUV Luminosity (erg s^{-1})		EUV Line Emission (counts)		
K	cm^{-3}		intrinsic	observed	130.3	131.2	132.6
5.200	59.403	5.94	34.38	30.22	2.4	2.3	3.9
5.225	59.167	3.44	34.28	30.07	1.5	1.5	3.4
5.250	58.968	2.18	34.22	29.98	1.0	1.2	3.3
5.275	58.758	1.34	34.16	29.91	0.8	1.0	3.3
5.300	58.611	0.96	34.15	29.87	0.7	1.0	3.3
5.350	58.355	0.53	34.17	29.84	0.9	1.2	3.6
5.400	58.251	0.42	34.28	29.85	1.8	1.9	4.2
5.450	58.273	0.44	34.45	29.85	5.5	5.2	8.1
5.500	58.656	1.06	34.94	30.08	7.9	8.9	9.1
5.550	59.074	2.78	35.42	30.33	15.6	26.2	16.3
5.600	59.573	8.77	35.98	30.64	29.4	78.9	28.5
5.650	60.091	28.96	36.57	30.96	51.9	212.7	44.3
5.700	60.544	82.05	37.07	31.25	86.4	501.6	60.0

FIGURE CAPTIONS

Figure 1. The EUV optical depths for the best fit two component model discussed in the text. Notice that the predicted optical depths are < 10 between 128 to 140 Å, a result of the unique combination of a low ISM column density and a highly ionized stellar wind (the contribution of each component is shown). The primary ions responsible for the various stellar wind opacity edges are indicated.

Figure 2. The two component best fit model to the ς Puppis ROSAT PSPC X-ray spectrum. The total and contribution of the EUV component are shown. This also illustrates the very high signal to noise PSPC observation.

Figure 3. A sample of EUV emission line models for several selected values of the EUV temperature. Note that the vertical axis (predicted EUVE counts) is variable. This shows that the continuum dominates the line emission for log $T_{EUV} < 5.2$. The continuum edge is due to FeVI and NeIV (see Fig. 1). This shows that the OV (135.9 Å) emission line is dominant for log T_{EUV} between 5.2 and 5.5, and above 5.5, the FeVIII (131.2 Å) line becomes the stronger.

Figure 4. The dependence of model EUV line strengths as a function of T_{EUV} for the strongest lines in the wavelength range of 130 to 140 Å. Of particular interest is the OV emission line, which is marginally detected in our EUVE observation, showing a relatively small range in T_{EUV}. Since the observed EUVE counts for the OV emission line is ≤ 16.8, and the other lines are < 10, the possible range in T_{EUV} is highly restricted.

Figure 5. The same as Figure 4, except showing the dependence on the normalized velocity location of the EUV source. The position of the X-ray source is indicated. The best fit EUV source is located at $V_{EUV} = 0.565$ which is seen to be located just below the X-ray source. We point out that as $v(r)/v_\infty$ decreases, the EUV emission measure and column density increases. This also shows that one cannot obtain a fit to the EUVE data for an EUV source above the X-ray source. Because of the observed line emission counts (see Fig. 4), the location of the EUV source is restricted to occur very close to the X-ray source.

Figure 6. A comparison of the best fit EUV/X-ray model with the observed EUVE SW spectrometer data (the best fit parameters correspond to log $T_{EUV} = 5.180$, see Table 1). The model counts are offset by 20 counts for comparison. The noise level of the observed spectrum illustrates the problem in establishing whether the OV emission line is a true detection or a null detection. However, since the model does predict only one strong line at 135.9 Å, and an observed 2.4 signal to noise feature is present at this wavelength, we suggest tat this may be a positive detection. In addition, statistically, between 130 to 140 Å, the observed spectrum indicates that there are more counts > 0 than there are < 0, as compared to other regions of the spectrum.

Figure 1. EUV Optical Depths for Best-Fit Model

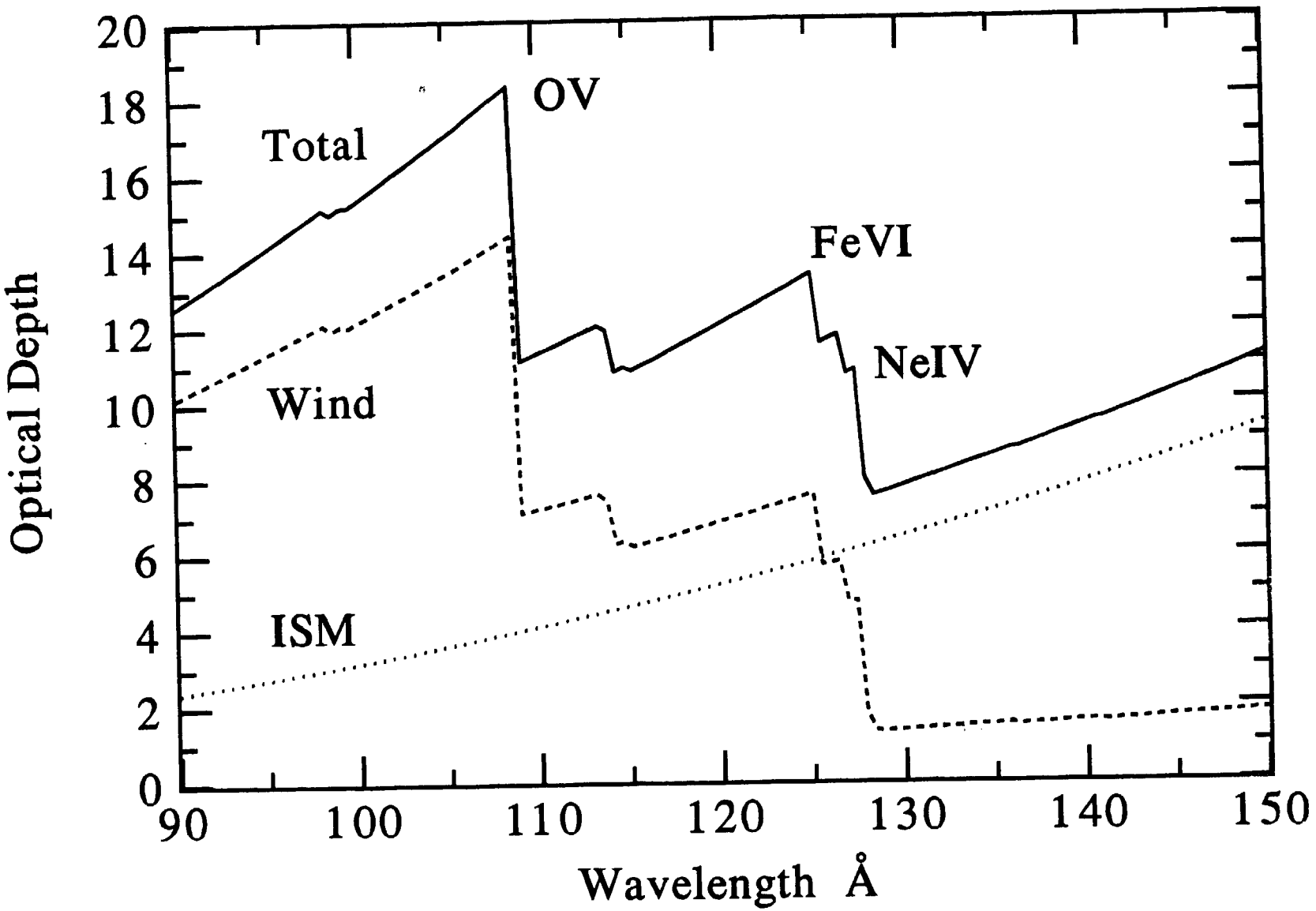

Figure 2. Comparison of Best-Fit Model to PSPC Spectrum

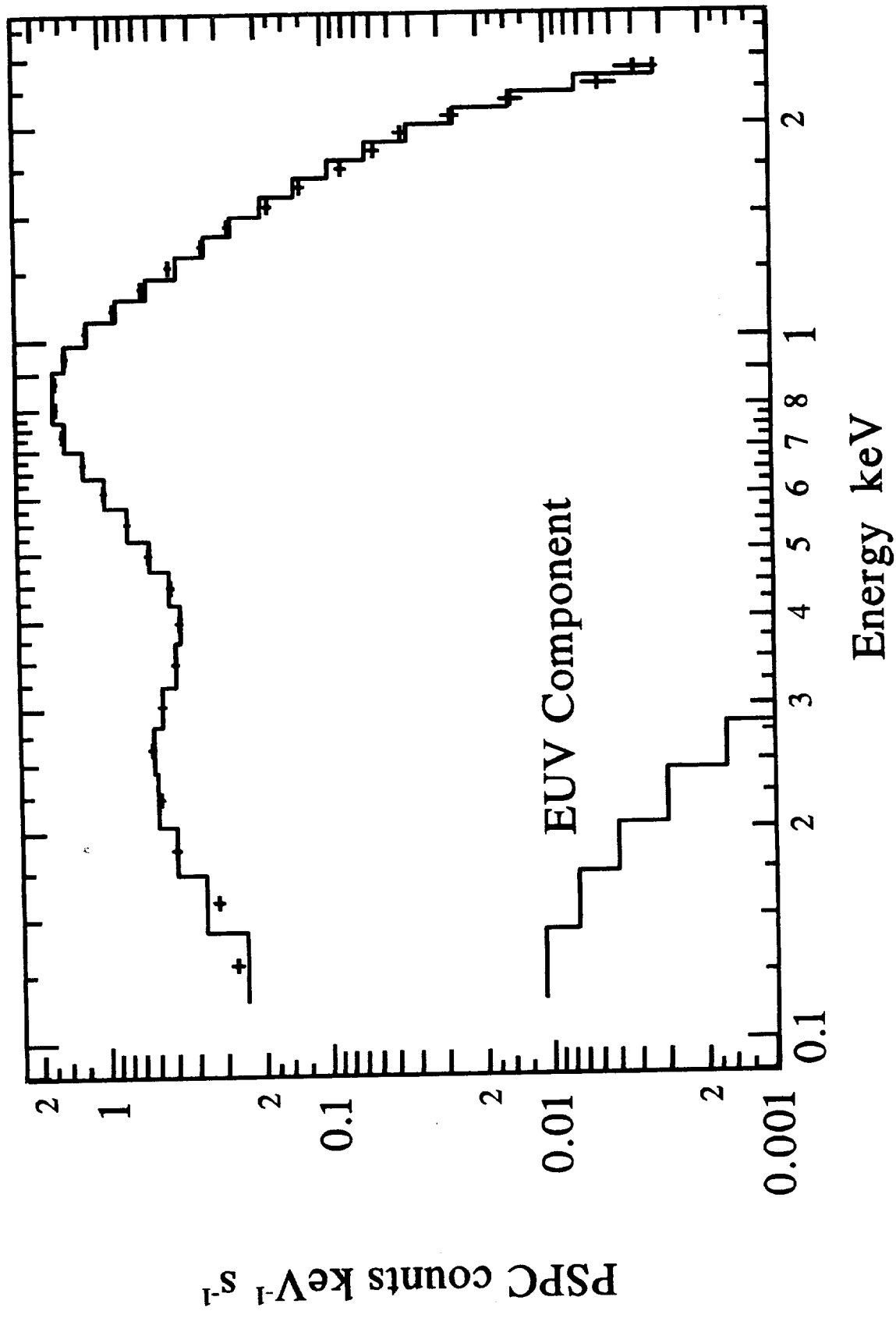

Figure 3. EUV Emission Line Models

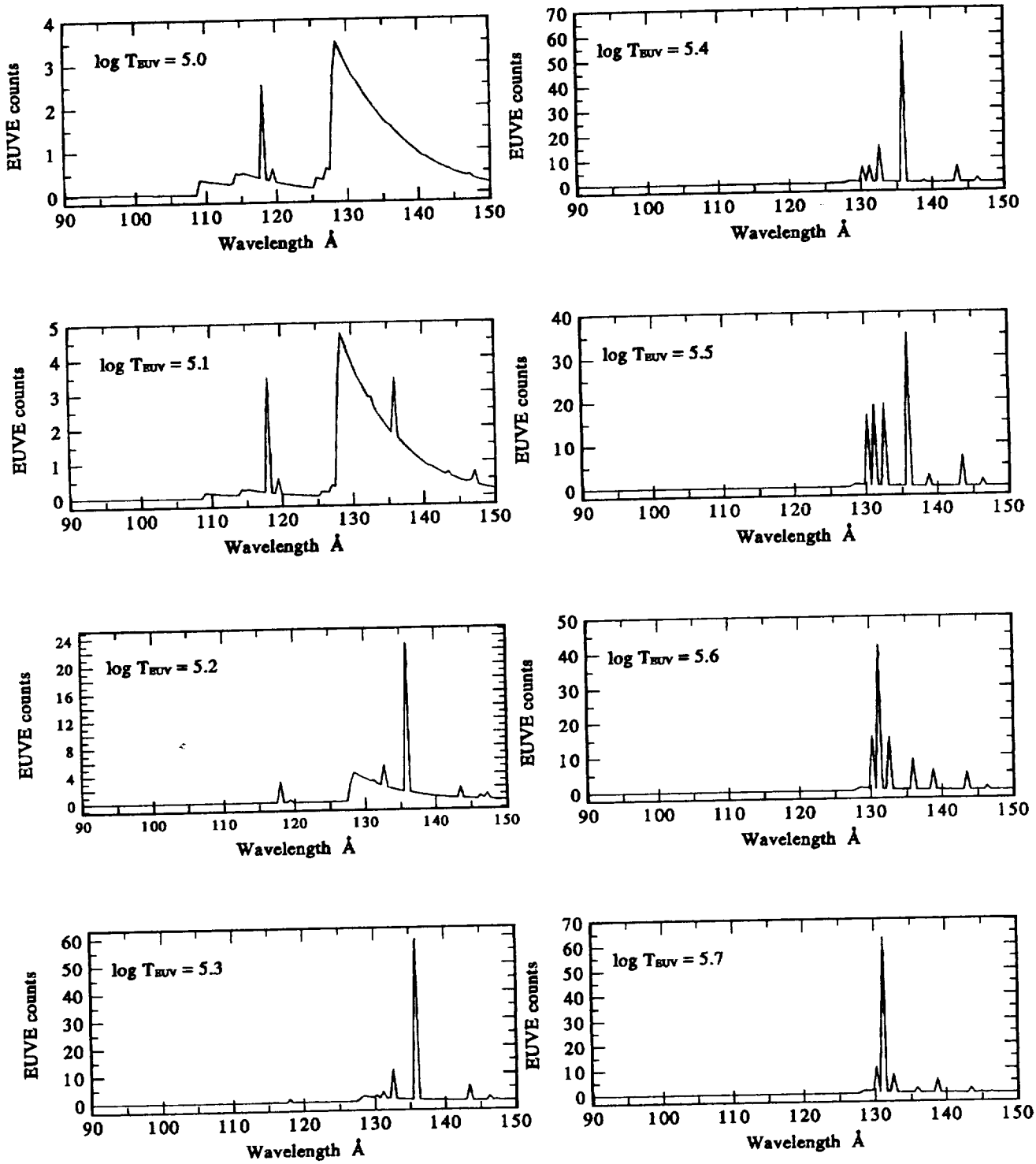

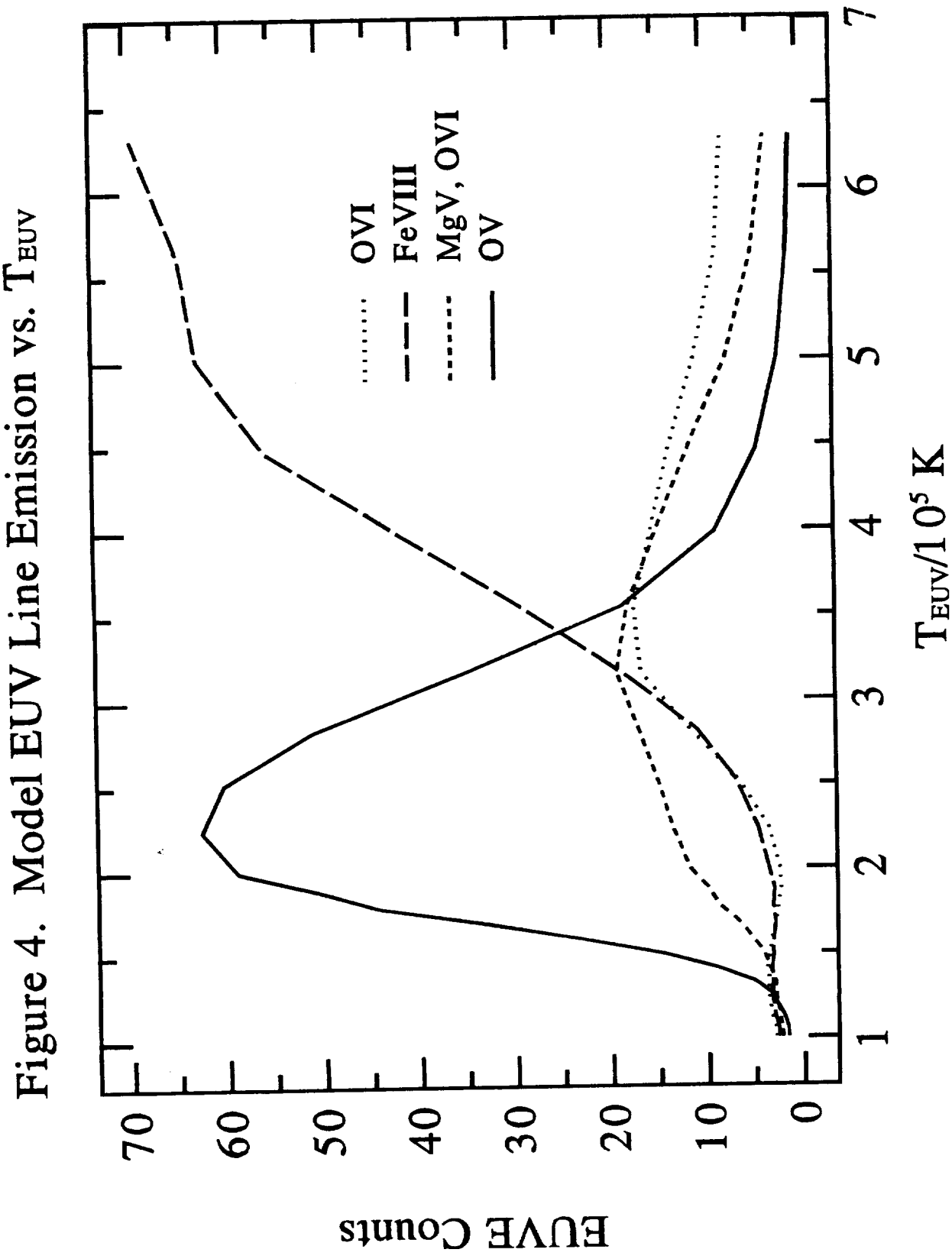

Figure 4. Model EUV Line Emission vs. T_{EUV}

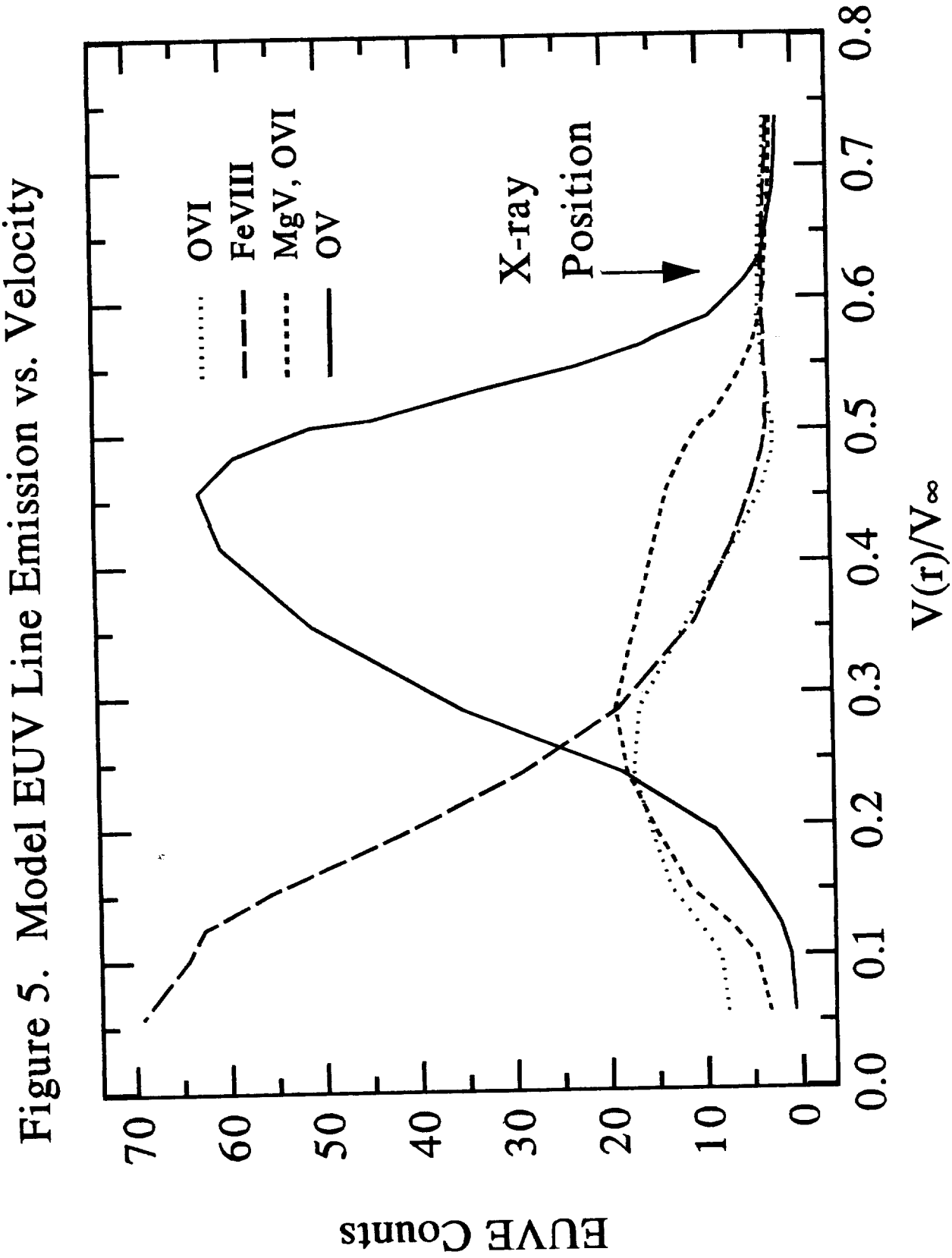

Figure 5. Model EUV Line Emission vs. Velocity

Figure 6. Comparison of Best-Fit Model with Observed Spectrum

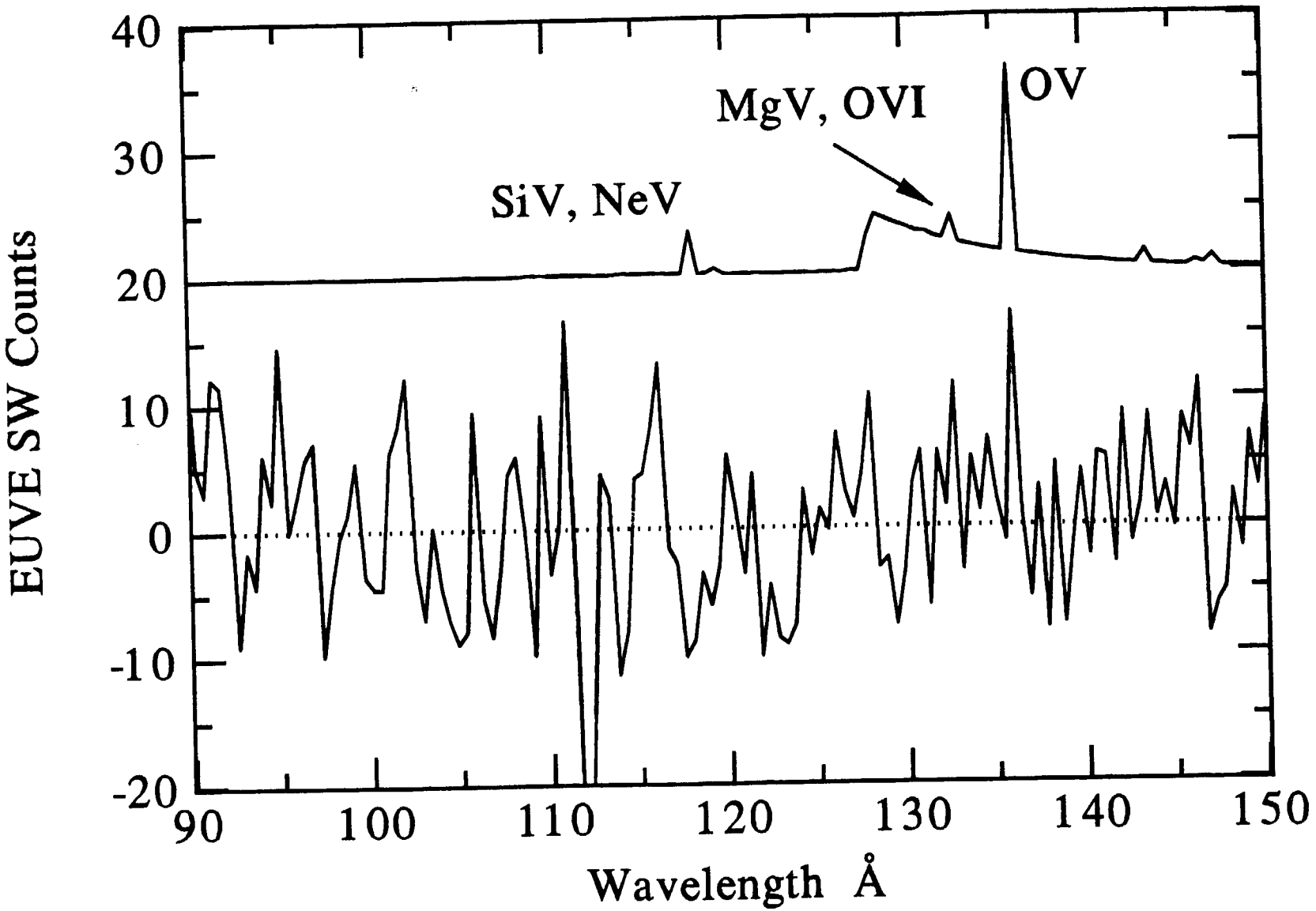

REPORT DOCUMENTATION PAGE

Form Approved
OMB No. 0704-0188

1. AGENCY USE ONLY *(Leave blank)*	2. REPORT DATE	3. REPORT TYPE AND DATES COVERED
	November 1996	Contractor Report

4. TITLE AND SUBTITLE

A Search for EUV Emission from the 04f Star Zeta Puppis

5. FUNDING NUMBERS

Code 691
Contract: S-30943-F

6. AUTHOR(S)

Dr. Wayne L. Waldron (Applied Research Corp.)
Dr. John Vallerga (Eureka Scientific, Inc.)

7. PERFORMING ORGANIZATION NAME(S) AND ADDRESS(ES)

Applied Research Corporation
8201 Corporate Drive, Suite 1120
Landover, MD 20785

8. PERFORMING ORGANIZATION REPORT NUMBER

R96-255

9. SPONSORING/MONITORING AGENCY NAME(S) AND ADDRESS(ES)

NASA Aeronautics and Space Administration
Washington, D.C. 20546-0001

10. SPONSORING/MONITORING AGENCY REPORT NUMBER

CR-199885

11. SUPPLEMENTARY NOTES

Technical Monitor: R. Oliverson, Code 691

12a. DISTRIBUTION/AVAILABILITY STATEMENT

Unclassified-Unlimited
Subject Category: 89
Report available from the NASA Center for AeroSpace Information,
800 Elkridge Landing Road, Linthicum Heights, MD 21090; (301) 621-0390.

12b. DISTRIBUTION CODE

13. ABSTRACT *(Maximum 200 words)*

We obtained a 140 ks EUVE observation of the 04f star, ς Puppis. Because of its low ISM column density and highly ionized stellar wind, a unique EUV window is accessible for viewing between 128 to 140 A, suggesting that this star may be the only O star observable with the EUVE. Although no SW spectrometer wavelength bin had a signal to noise greater than 3, a bin at 136 Å had a signal to noise of 2.4. This bin is where models predict the brightest line due to OV emission should occur. We present several EUV line emission models. The models were constrained by fitting the ROSAT PSPC X-ray data and our EUVE data. If the OV emission is real, the best fits to the data suggest that there are discrepancies in our current understanding of EUV/X-ray production mechanisms. In particular, the emission measure of the EUV source is found to be much greater than the total wind emission measure, suggesting that the EUV shock must produce a very large density enhancement. In addition, the location of the EUV and X-ray shocks are found to be separated by ~0.3 stellar radii, but, the EUV emission region is found to be ~400 times larger thatn the X-ray emission region. We also discuss the implications of a null detection and present relevant upper limits.

14. SUBJECT TERMS

EUVE, X-rays, O Stars, Zeta Puppis

15. NUMBER OF PAGES

16

16. PRICE CODE

17. SECURITY CLASSIFICATION OF REPORT	18. SECURITY CLASSIFICATION OF THIS PAGE	19. SECURITY CLASSIFICATION OF ABSTRACT	20. LIMITATION OF ABSTRACT
Unclassified	Unclassified	Unclassified	Unlimited